23PM2E-02

Analysis of Path Gain Inside Tunnels Based on FDTD and Ray Tracing Methods

Gilbert Siy Ching #1, Kensuke Tsuda #2, Yukiko Kishiki #3

Electromagnetic Analysis Team, Kozo Keikaku Engineering Inc.
4-5-3 Chuo, Nakano-ku, Tokyo, 164-0011, Japan
1 ching-g-siy@kke.co.jp
2 kensuke-tsuda@kke.co.jp
3 y-sanoh@kke.co.jp

***Abstract*—Tunnel simulations are important to study the propagation mechanisms inside tunnels. In this work, FDTD and ray tracing methods are used to simulate the path gain for 2 transmitters located inside a rectangular concrete tunnel. The applicability of ray tracing is analyzed by comparing it with results from FDTD. FDTD results with and without object inside the tunnel show that at distances far from the transmitter, the path gain can be approximated with a constant attenuation.**

I. Introduction

Tunnel communications include personal communications, vehicle to vehicle communications and data exchange between trains and stations for subway tunnels. According to the Japanese Ministry of Internal Affairs and Communications, one of its aims is to be able to use broadband wireless services for trains at the 400 MHz band [1]. Measurement campaigns in the literature range from a combination of narrowband to wideband, and non-directional to directional measurements [2] - [3], because there is a need to study the behavior of radiowave propagation inside tunnels. But not all locations can be easily measured especially if the tunnel is already in operation, so simulations are equally important. Tunnel simulations usually use modal analyses [4] or ray tracing based techniques [5]-[7]. With the improvement of computer resource, it is also possible to use electromagnetic simulation techniques such as the finite difference time domain (FDTD) method. Previous work was done for a 100 m long tunnel [8]. The results showed that FDTD and ray tracing methods are similar for a rectangular tunnel with and without objects. In this work, a longer and more realistic tunnel operating at 400 MHz is compared between the 2 methods. Furthermore, the attenuation constant of path gain is also analyzed.

II. Methodology

A. Simulation Geometry

Fig. 1 shows the locations of transmitters (Tx) and receivers (Rx) inside the tunnel while Table I lists down the simulation parameters for the FDTD and ray tracing methods. The frequency used in this work was set to 400 MHz in preparation for broadband wireless services for transportation systems. The simulation model is a 1010 m long rectangular concrete tunnel, with cross section of 3.8 m x 4.3 m or 5.1λ x 5.7λ where λ is the wavelength. The front and back of the tunnels are open. Two Tx cases are used, one located at the center (TxCenter) and another one located 0.88 m to the left from the center (TxSide). Both Tx heights are at 2.82 m, and situated 10 m into the tunnel. Two Rx routes are located 0.717 m to the right from the center to represent one side of a train track. One route has a height of 1.47 m (RxLow) while the other has a height

TABLE I
Simulation parameters

Parameter	Value
Tunnel size	1010 m (length), 3.8 m (width) 4.3 m (height)
Wall thickness	10 cm
Tunnel material	concrete (permittivity: $5 - j0.1$)
Frequency	400 MHz
Wavelength	0.749 m
Tx antenna	vertically polarized halfwave dipole
Tx locations	TxCenter [10,0,2.82]m; TxSide [10,0.88,2.82]m;
Rx antenna	vertically polarized omni antenna
Rx locations	RxLow [x,-0.717,1.47]m; RxHigh [x,-0.717,2.82]m;
FDTD grid size	0.020 to 0.024 m
FDTD convergence criteria	40 dB below excitation value
Ray tracing condition	up to 10 reflections
Ray tracing Rx spacing	1 m

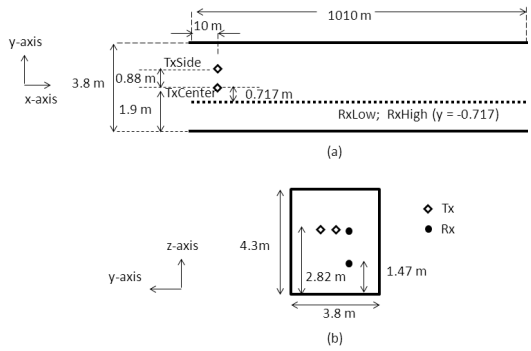

Fig. 1. Illustration of simulation geometry. (a) Top view. (b) Front view.

of 2.82 m (RxHigh). A vertically polarized halfwave dipole is used at Tx, while a vertically polarized omnidirectional antenna is used at Rx.

B. FDTD Method

With the advancement of computer resource, it is now possible to solve electrically large models using electomagnetic simulation techniques such as FDTD within a reasonable time. FDTD solves Maxwell's equations in time domain as opposed to frequency domain. To correctly represent the change of simulation values in FDTD, the simulation geometry needs to be divided into discrete segments or grids which must be at least 10 times smaller compared to the wavelength and also smaller than the smallest dimension in the geometry. These segments are then used as basis to represent the electric or magnetic fields based on the Yee cell. After an excitation is applied, the fields are continuously computed until the fields have decayed to a very small value. In this simulation, a value of 40 dB below the excitation power was used. The grid size ranges from 0.020 to 0.024 m along the 1010 m x 4 m x 4.5 m simulation space.

The FDTD software used in this work is capable of using graphic processing units (GPU) in a computer cluster [9]. To shorten the simulation time, Tokyo Institute of Technology's supercomputer TSUBAME 2.0 was used [10]. 8 hosts were used for the simulation, with each host having 8 cores, CPU speed of 3 GHz and 3 GPUs (Tesla M2050). With these specifications, the simulations finished in 30 minutes. The FDTD results are used as the basis for comparison with the ray tracing results.

C. 3D Ray Tracing Method

For the ray tracing results, a full 3D ray tracing software based on the imaging method was used [11]. At first, rays from Tx to Rx are searched depending on the locations of the Tx, Rx, geometry and number of maximum desired reflections, diffractions and/or transmissions. Once the rays are known, the electric field of each ray at Rx are calculated based on the Fresnel coefficients and uniform theory of diffraction [12]. The combination of the individual electric fields with the Rx antenna information then gives the received power at Rx. The ray tracing simulation was run in a personal computer with 8 cores, 16 Gbytes of RAM and CPU speed of 3.5 GHz.

III. Results

A. Path Gain Comparison for FDTD and Ray Tracing

Figs. 2 to 5 show the path gain comparisons along the tunnel depth, for the 2 Tx and 2 Rx routes using the 2 simulation methods. Path gain is defined as the received power normalized to the transmit power. The solid line represents the FDTD results, while the dashed line represents the ray tracing results. The dotted line is from Eq. (1) and will be discussed in the next subsection. For all cases, both FDTD and ray trace methods produce similar results until a tunnel depth normalized to wavelength of around 200 - 300. The ray tracing results also accurately simulate values near the Tx where there are rapid fluctuations.

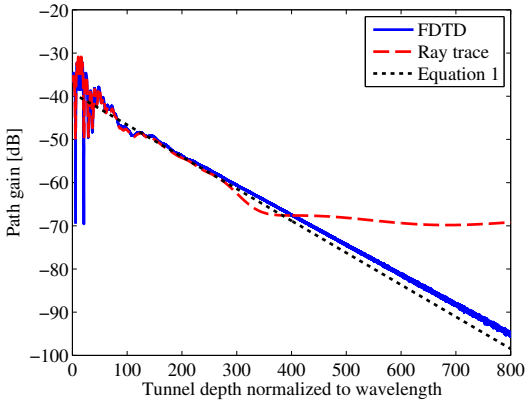

Fig. 2. Path gain comparison of FDTD and ray tracing for TxCenter and RxLow.

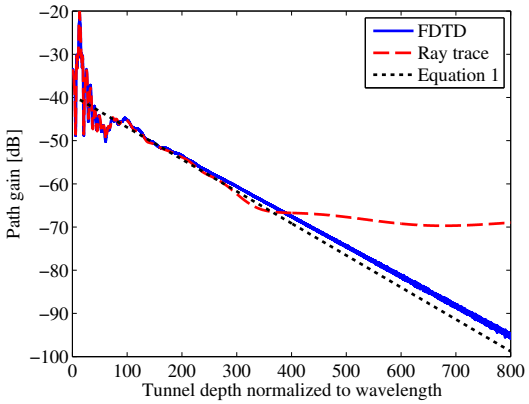

Fig. 3. Path gain comparison of FDTD and ray tracing for TxCenter and RxHigh.

B. Attenuation Constant in Dominant Mode Region

A tunnel can be thought of as an oversized waveguide. Close to Tx, field consists of many modes and interact to produce rapid fluctuations, while at farther distances from Tx, the fields will be dominated by only a few principal modes, or a single dominant mode [13]. Figs. 2 and 3 show that for TxCenter,

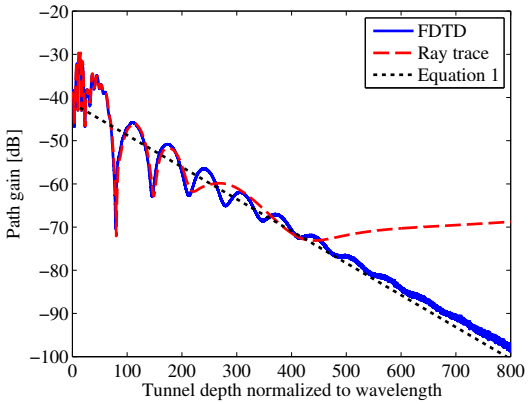

Fig. 4. Path gain comparison of FDTD and ray tracing for TxSide and RxLow.

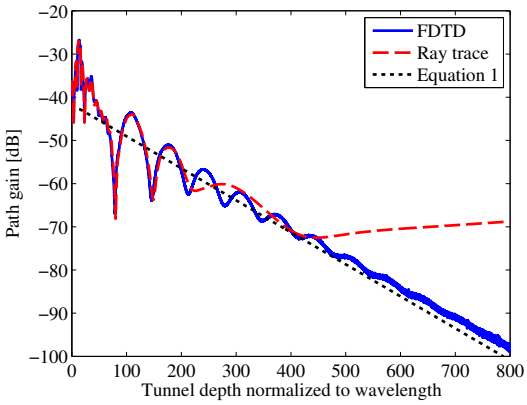

Fig. 5. Path gain comparison of FDTD and ray tracing for TxSide and RxHigh.

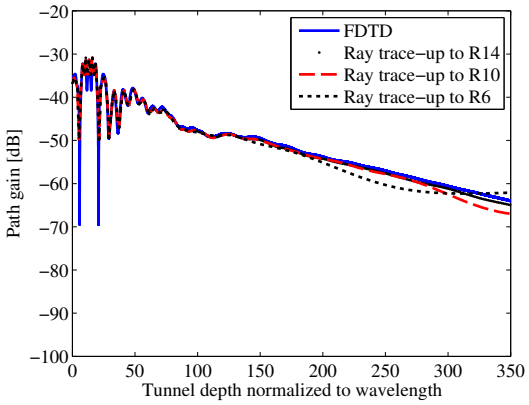

Fig. 6. Comparison of FDTD and ray tracing result for different number of maximum reflections for TxCenter and RxLow.

the dominant mode region starts at a tunnel depth normalized to wavelength of around 100. Figs. 4 and 5 on the other hand show that for TxSide, the dominant mode region starts at a farther distance from Tx, at around 500. This difference is due to the location of the Tx wherein the non principal modes for TxCenter cancel each other more easily due to its symmetry.

The attenuation constant in the dominant mode region can be approximated with the following equation [14]

$$\alpha = K\lambda^2 \left(\frac{1}{a^3\sqrt{\epsilon_r - 1}} + \frac{\epsilon_r}{b^3\sqrt{\epsilon_r - 1}} \right) \quad (1)$$

where α is the attenuation constant in dB/m. K is a coefficient depending on the shape of the cross section of the tunnel. For rectangular cross section, $K = 4.34$. ϵ_r is the relative permittivity of the tunnel's material which in this case is concrete, while a and b are the width and height of the tunnel cross section respectively.

Table II compares the attenuation constant by using Eq. (1), and by fitting a line to the FDTD result. Since Eq. (1) does not depend on the location of Tx and Rx, the attenuation constants are the same for all cases. Even if these values do not change, it differs only by 6 dB for a 1km distance compared to the attenuation constants from FDTD results. Eq. (1) is therefore accurate in predicting the attenuation constants in the dominant mode region. To illustrate this graphically, Eq. (1) is plotted on Figs. 2 to 5 represented by the dotted lines.

TABLE II
ATTENUATION CONSTANT IN DECIBELS/M

Simulation Model	FDTD	Eq. (1)
TxCenter, RxLow	-0.0928	-0.0989
TxCenter, RxHigh	-0.0924	-0.0989
TxSide, RxLow	-0.0936	-0.0989
TxSide, RxHigh	-0.0930	-0.0989

C. Effects of Number of Reflections in Ray Tracing Method

Fig. 6 plots again the path gain for TxCenter and RxLow. In addition to the FDTD result, this figure now includes ray tracing results for a maximum number of reflection of 6, 10 and 14. As the figure shows, more reflections are needed so that the results will be closer to the FDTD results.

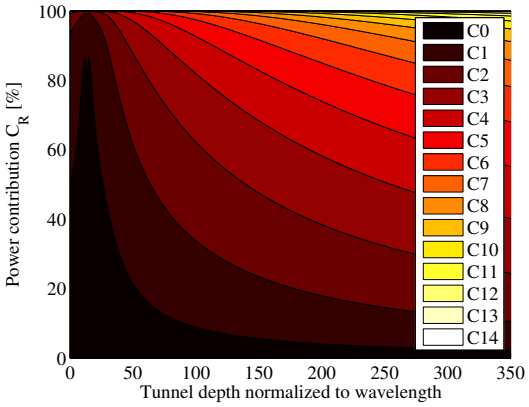

Fig. 7. Power contribution of each respective reflections of the ray tracing method for TxCenter and RxLow.

Based on the region where the FDTD and ray tracing methods are similar, Fig. 7 plots the power contribution of each respective reflection, C_R to the total path gain of the ray tracing method based on the following equation

$$C_R = \frac{P_R}{\sum_{R'=0}^{14} P_{R'}} \quad (2)$$

where P_R means the path gain at R number of reflections only, and the denominator is the total path gain. For example, C_0 means the power contribution for 0 reflections (line-of-sight ray), C_1 means the power contribution for 1 reflection rays only, and so forth. For Rx locations near Tx, as few as 3 reflections are enough. But as Rx locations move farther away from Tx, higher number of reflections have more significant contribution to the overall level. Fig. 8 is another way to interpret the results of Fig. 7. This figure shows the number of maximum reflections needed to obtain a desired percentage of total path gain for this specific case. As expected, when the tunnel gets longer, more reflections are needed.

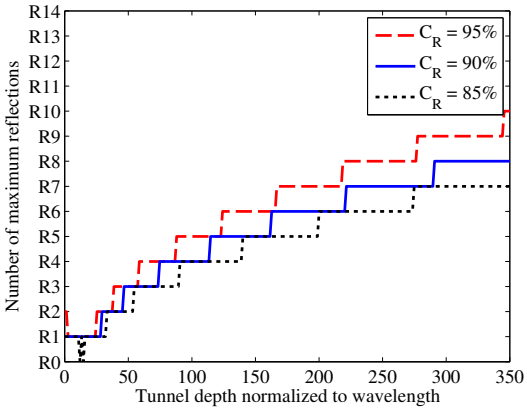

Fig. 8. Number of maximum reflections needed to get desired power contribution of total path gain of the ray tracing method for TxCenter and RxLow.

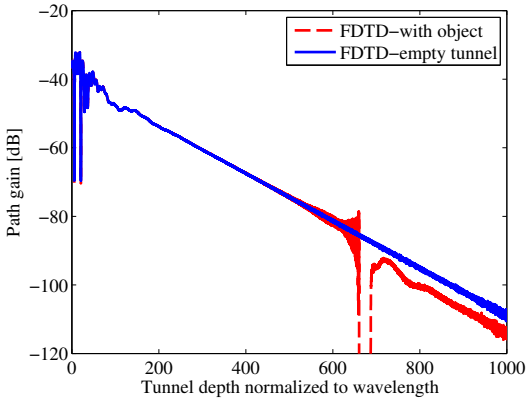

Fig. 9. Comparison of FDTD results for tunnel with and without object (empty tunnel) for TxCenter and RxLow.

D. Effects of Object Inside Tunnel

In this subsection, an object representing a train is included inside the tunnel. The size of the object is 2.8 x 20 m with a height of 2 m. The object is located 485 m (or 646.7 when normalized to the wavelength) away from Tx and is placed symmetrically along the center. The material of the object is set to copper with permittivity of 1 and conductivity of 5.96 x 10^7 S/m. The simulations also finised in 30 minutes. Fig. 9 shows the path gain from FDTD for TxCenter and RxLow. The solid line shows the empty tunnel result while the dashed line shows the result with object inside the tunnel.

For FDTD results with object, since RxLow is lower than the height of the object, there is no value from 646.7 to 673.3. Up to until a tunnel depth normalized to wavelenth of 500, FDTD results with object is similar to FDTD results without object, and also exhibits a dominant mode region. At locations before the object, standing waves occur due to the incoming wave from Tx and reflections from the front of the object. At locations after the object, the dominant region again reappears but the path gain is shifted down by around 5 dB as compared to the FDTD result without object. For the other Tx and Rx cases, it also exhibits a similar behavior.

IV. Conclusion

FDTD and ray tracing results were compared for an empty rectangular concrete tunnel. Near Tx, fields fluctuate rapidly due to the interaction of many modes. At farther distances from Tx, the fields will be dominated by only a few principal modes. For TxCenter, this dominant region starts at a tunnel depth normalized to wavelength of around 100, while at TxSide, it starts at 500. For the ray tracing results to be similar to the FDTD results up to the dominant region, higher number of reflections must be included. In the dominant mode region, the attenuation constant of the path gain can be approximated by a line independent of the location of Tx and Rx. This attenuation constant is shifted downwards when objects are inside the tunnel. With the advancement of computer resource, it is now possible to solve electrically large models using FDTD within a reasonable time. In our case, with the use of computer clusters, the simulations finished in 30 minutes. For the same simulation space, FDTD also has the advantage of being able to solve complex geometries at the same time.

References

[1] Frequency reorganization action plan. Ministry of Internal Affairs and Communications. [Online]. Available: http://www.tele.soumu.go.jp/j/adm/freq/search/saihen/index.htm

[2] A. G. Emslie, R. L. Lagace, and P. F. Strong, "Theory of the propagation of UHF radio waves in coal mine tunnels," *IEEE Trans. Antennas Propag.,* vol. AP-23, pp. 192-205, Mar. 1975.

[3] G. S. Ching, M. Ghoraishi, M. Landmann, N. Lertsirisopon, J. Takada, T. Imai, I. Sameda, and H. Sakamoto, "Wideband polarimetric directional propagation channel analysis inside an arched tunnel," *IEEE Trans. Antennas Propag.,* vol. 57, no. 3, pp. 760-767, Mar. 2009.

[4] J. M. Molina-Garcia-Pardo, M. Liénard, A. Nasr, and P. Degauque, "On the possibility of interpreting field variations and polarization in arched tunnels using a model for propagation in rectangular or circular tunnels," *IEEE Trans. Antennas Propag.,* vol. 56, no. 4, pp. 1206-1211, Apr. 2008.

[5] D. Didascalou, T. Schäfer, F. Weinmann, and W. Wiesbeck, "Ray-density normalization for ray-optical wave propagation modeling in arbitrarily shaped tunnels," *IEEE Trans. Antennas Propag.,* vol. 48, no. 9, pp. 1316-1325, Sep. 2000.

[6] T. Imai, "Prediction of propagation characteristics in tunnels using ray-tracing method," *IEICE Trans. Commun. (Japanese Edition),* vol. J85-B, no. 2, pp. 216-226, Feb. 2002.

[7] Y. Kishiki, J. Takada, G. S. Ching, H. Takao, Y. Sugihara, S. Matsunaga, and F. Uesaka, "Implementation of Reflection on Curved Surfaces and Physical Optics in Ray Tracing for Tunnel Propagation," *IEICE Trans. Electron.,* vol. E96-C, no.1, pp. , Jan. 2013.

[8] G. S. Ching, K. Tsuda, and Y. Kishiki, "Comparison of Propagation Characteristics Using Ray Tracing Method and FDTD for Wireless Services inside Tunnels," *IEICE Technical Report,* AP2012-37, July 2012.

[9] XFdtd, Remcom, Inc. [Online]. Available: http://www4.kke.co.jp/network/xfdtd/

[10] Tsubame 2, Tokyo Institute of Technology. [Online]. Available: http://www.gsic.titech.ac.jp/en/tsubame2

[11] RapLab, Kozo Keikaku Engineering, Inc. [Online]. Available: http://www4.kke.co.jp/raplab/

[12] R. G. Kouyoumjian and P. H. Pathak, "A uniform geometrical theory of diffraction for an edge in a perfectly conducting surface," *Proc. IEEE,* vol. 62, pp. 1448-1461, November 1974.

[13] D. G. Dudley and P. Yuan, "System identification for wireless propagation channels in Tunnels," *IEEE Trans. Antennas Propag.,* vol. 53, no. 8, pp. 2400-2405, Aug. 2005.

[14] Y. Yamaguchi, T. Abe, and T. Sekiguchi, "On the approximate equation for the attenuation constant in tunnels with arbitrary cross section," *IEICE Trans. Commun. (Japanese Edition),* vol. J67-B, no. 3, pp. 352-353, Mar. 1984.